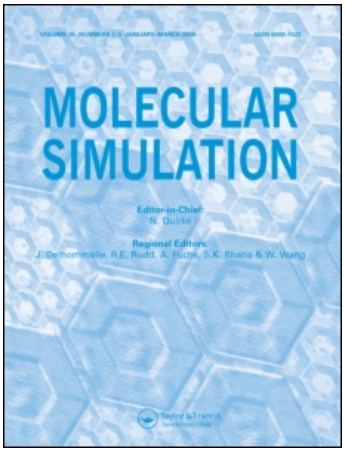

Molecular Simulation
Publication details, including instructions for authors and subscription information:
http://www.informaworld.com/smpp/title~content=t713644482

Full-band quantum transport based simulation for carbon nanotube field effect transistor from chirality to device performance

Y. Tao[a]; J. He[a]; X. Zhang[a]; T. Y. Man[b]; M. Chan[b]
[a] School of Computer and Information Engineering, Peking University Shenzhen Graduate School, Shenzhen, People's Republic of China [b] Department of Electronic and Computer Engineering, The Hong Kong University of Science and Technology, Kowloon, Hong Kong

To cite this Article Tao, Y. , He, J. , Zhang, X. , Man, T. Y. and Chan, M.(2008) 'Full-band quantum transport based simulation for carbon nanotube field effect transistor from chirality to device performance', Molecular Simulation, 34: 1, 73 — 81
To link to this Article: DOI: 10.1080/08927020701730377
URL: http://dx.doi.org/10.1080/08927020701730377

Molecular Simulation
Vol. 34, No. 1, January 2008, 73–80

Taylor & Francis
Taylor & Francis Group

Full-band quantum transport based simulation for carbon nanotube field effect transistor from chirality to device performance

Y. Tao[a], J. He[a]*, X. Zhang[a], T.Y. Man[b] and M. Chan[b]

[a]*School of Computer and Information Engineering, Peking University Shenzhen Graduate School, Shenzhen 518055, People's Republic of China;* [b]*Department of Electronic and Computer Engineering, The Hong Kong University of Science and Technology, Clearwater Bay, Kowloon 999077, Hong Kong*

(Received 11 July 2007; final version received 6 October 2007)

Carbon nanotube field effect transistor (CNFET) may be one of the most promising alternatives to silicon complementary metal-oxide-semiconductor (CMOS) due to its unique advantages. The predicted dependences of band structure and device performance on chirality of carbon nanotube (CNT) and device structure have been studied in this paper by the means of a full-band based quantum transport simulator, ALTRAS-CNFET. Including the modification of curvature effect, the band structure of CNT is obtained by the tight-binding approach. The self-consistent solution of Schrödinger–Poisson equation groups is employed to calculate the direct tunneling gate current in the coaxial CNFET radial direction under cylindrical coordinates. The electrical characteristic in the coaxial CNFET channel direction is also computed based on the ballistic transport mechanism.

Keywords: carbon nanotube (CNT); carbon nanotube field effect transistor (CNFET); band structure; quantum transport; molecular electronics; molecular simulation

1. Introduction

For years, while the semiconductor industry has been projecting Moore's law and performance scaling to upcoming CMOS generations, the industry has also been warning about "Red Brick Walls" of processes, materials, and physics which may block this seemingly unstoppable path to smaller, faster, cheaper devices and circuits [1]. In order to breakthrough these "Red Brick Walls", the research needs for extending CMOS technology up to sub-10 nm regime included new materials and device designs required to overcome these transistor scaling limitations. In particular, the increased efforts in molecular electronics for improved channel electrostatics and enhanced channel transport result in that we can produce billions of devices/transistors very cheaply in a beaker. There exist three main technological areas within molecular electronics, organic electronics, nanotube devices, and single molecule devices. Among them, the nanotubes are unique nanostructures with a number of advantages such as ideal scalability, tunable band gap, strong covalent bonding, possible ballistic transport, high thermal conductivity and self-assembly [2–4].

To study the compelling properties and apply them to devices adequately, the band structure characteristics and the device configuration optimization are critical for carbon nanotube (CNT) transistor application. In recent years, a lot of efforts have been devoted to CNT band structure modeling, and some important results have been obtained [4–8]. For example, a detailed derivation of the energy dispersion relation has been obtained by Saito *et al.* based on a tight-binding approximation [5–6]. At the same time, carbon nanotube field effect transistors (CNFETs) have been fabricated in various CNT configurations and their performances have been studied in detail [9–26]. Although CN FETs and circuits have already been demonstrated, the conductance mechanism through the nanotubes as well as the contact is not yet well understood. To ensure scalability, the electrostatic properties of an individual nanotube as well as an array of nanotubes must be explored. For CNT transistor optimization and circuit performance benchmark, a complete study from the nanotube chirality and energy band structure to device characteristics is really needed either from the theory base or from the engineering practice. A little attention, however, has been devoted to the aspect so far.

In this paper, a full-band based quantum transport simulator for CNFET engineering from chirality to device performance, ALTRAS-CNFET, is developed and further used to test CNFET performance. The tight-binding approach is followed to derive a simple model including the modification of curvature effect. Based on the resultant band gap and density of states, we present an implementation of the self-consistent Schrödinger–Poisson

*Corresponding author. Email: jinhe@ime.pku.edu.cn

ISSN 0892-7022 print/ISSN 1029-0435 online

DOI: 10.1080/08927020701730377
http://www.informaworld.com

equations and the electrical characteristics of the CNFETs. From the simulator, the direct tunneling gate current in the coaxial CNFET radial direction under cylindrical coordinates is calculated [20]. The electrical characteristics in the coaxial CNFET channel direction are also computed based on the ballistic transport mechanism [21–23]. As a consequence, we have directly obtained CNFET electronic structures such as E–K relationship and electrical characteristics such as the dependence of the drain current and the direct tunneling gate current on gate voltage from this powerful simulator, which does not require highly computational resources and time consumption. The results can be used to design and optimize the electrical characteristics of CNFETs. Finally, we would like to stress that the methods and technologies used in this paper can be easily extended to other molecule based devices to model electron transport characteristics and their performance, thus, it is useful for us to simulate the quantum based transport mechanisms of the molecular devices and predict the corresponding device optimization.

2. Description of the simulation process

2.1 Calculation of energy-band structure of CNT

Following [10], the CNT is treated as a rolled-up graphite sheet and assumed a single pi orbit per carbon atom. The three vectors in the tight-binding model, however, are not in the same plane due to the curvature effect. Taking zigzag CNT $(n, 0)$ as an illustration, a sketch for denoting the changes of vectors according to the curvature effect is shown in Figure 1, where (a) is the cross section along the line 0–1 parallel to the paper plane and (b) is the corresponding graphite crystal lattice.

It is obvious that the C—C bond is bent due to the curvature effect, as shown in Figure 1(a), arc (0, 1) being the C—C bonding distance. However, the magnitude of the vector $\vec{R}_1$ is no longer the C—C bonding distance but the distance between 0 and 1. The changes on $\vec{R}_2$ and $\vec{R}_3$ are same as that of $\vec{R}_1$. The number of carbon atoms in the cross section is n and the angle between O1 and O2 is tagged as α, which can be obtained as $\alpha = \sqrt{3}a_0/r$ where a_0 is the C—C bonding distance and r is the diameter of the CNT with $r = \sqrt{3}na_0/\pi$. The angle β shown in Figure 1 (a) is half of α, i.e. $\beta = \alpha/2$. As a result, considering the curvature effect, the three vectors can be modified as [5–6]

$$\begin{cases} \vec{R}_1 = \frac{1}{2}a_0\vec{i} + r\sin\alpha\vec{j} - 2r\sin^2\frac{\alpha}{2}\vec{k} \\ \vec{R}_2 = \frac{1}{2}a_0\vec{i} - r\sin\alpha\vec{j} - 2r\sin^2\frac{\alpha}{2}\vec{k}. \\ \vec{R}_3 = a_0\vec{i} \end{cases} \tag{1}$$

Putting the three vectors into the tight-binding approach with the periodic boundary condition around

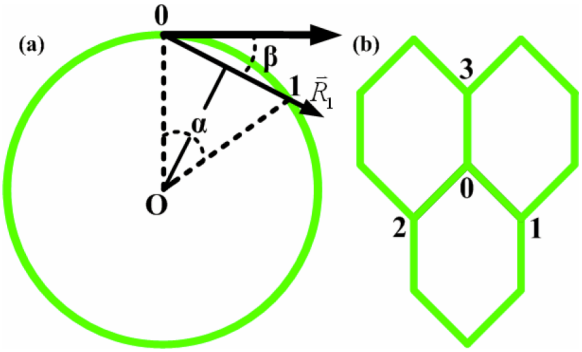

Figure 1. A sketch for denoting the changes of vectors according to curvature effect, where (a) is the cross section along the line 0–1 parallel to the paper plane and (b) is the corresponding graphite crystal lattice.

the circumference $n\sqrt{3}ka_0 = 2\pi q$, where k is the wave vector component along the circumference direction and q is an integer, the band structure of zigzag CNT $(n, 0)$ containing the modification of curvature effect is written as

$$E(k) = \pm t\left[1 \pm 4\cos(q\sin\alpha)\cos\left(\frac{3}{2}a_0k + 2r\sin^2\frac{\alpha}{2}k\right) + 4\cos^2(q\sin\alpha)\right]^{1/2}. \tag{2}$$

Employing the same method on the semiconducting chiral CNT specified by (n, m), the corresponding three vectors are as follows

$$\begin{cases} \vec{R}_1 = r\sin\alpha\vec{i} - 2r\sin^2\frac{\alpha}{2}\vec{k} \\ \vec{R}_2 = -r\sin\frac{\alpha}{2}\vec{i} + \frac{\sqrt{3}}{2}a_0\vec{j} - 2r\sin^2\frac{\alpha}{4}\vec{k} \\ \vec{R}_3 = -r\sin\frac{\alpha}{2}\vec{i} - \frac{\sqrt{3}}{2}a_0\vec{j} - 2r\sin^2\frac{\alpha}{4}\vec{k}. \end{cases} \tag{3}$$

The amendatory energy band expression is obtained

$$E(k) = \pm t\left[1 + 4\cos\left(\frac{\sqrt{3}a_0k}{2}\right)\cos\left(q\sin\frac{\alpha}{2} + q\sin\alpha\right) + 4\cos^2\left(\frac{\sqrt{3}a_0k}{2}\right)\right]^{1/2}. \tag{4}$$

The nanotube density of states is given by [24]

$$D_p(E) = \frac{8}{3\pi V_\Pi a_0}\frac{E}{\sqrt{E^2 - \Delta_p^2}} \tag{5}$$

where V_Π is the C—C bonding energy and Δ_p is the equilibrium conduction band minimum of the pth sub-band.

Using (2) or (4) and (5), the electron energy-band structure of CNT can be directly obtained in the ALTRAS-CNFET, and the results are employed in the following simulation steps.

2.2 Gate tunneling current in the radial direction of CNFET

The device geometry diagram of a coaxial CNFET with high-K dielectric is shown in Figure 2 for the simulation. Using the conventional central difference method and the resultant band gap and density of states, the simulator solves the Schrödinger and Poisson equations self-consistently in the radial direction under the cylindrical coordinates including the effect of wave function penetration into the gate electrode.

It is evident that the characteristic in every direction in the cross section is similar, so the one-dimensional form of Poisson equation under cylindrical coordinates is just focused in this study, the general form of which can be expressed as

$$\frac{\partial}{\partial r}\left(\varepsilon(r)\frac{\partial \Phi}{\partial r}\right)+\frac{\varepsilon(r)}{r}\frac{\partial \Phi}{\partial r}=-q\cdot\rho(x). \tag{6}$$

Based on the same principle, the one-dimensional form of the time-independent effective mass Schrödinger equation under the cylindrical coordinates is written as

$$\frac{\partial}{\partial r}\left(\frac{1}{m^*(r)}\frac{\partial \Psi(r)}{\partial r}\right)+\frac{1}{m^*(r)}\frac{1}{r}\frac{\partial \Psi(r)}{\partial r} =(q\phi(r)-E)\Psi(r). \tag{7}$$

The conventional central difference method is used to convert Equations (6) and (7) into the discrete format,

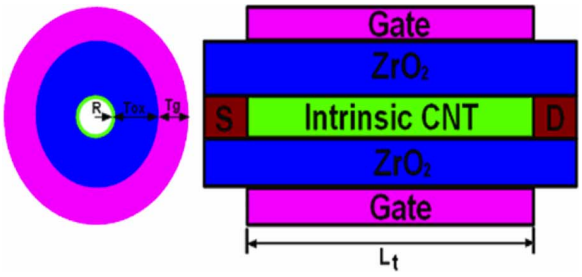

Figure 2. A physical diagram of a coaxial CNFET with length 20 nm and high-K dielectric.

which can be implemented immediately by the simulator.

$$\left(\frac{\varepsilon_{k-0.5}}{\Delta\bar{r}_k\cdot\Delta r_{k-1}}-\frac{\varepsilon_k}{2r_k\Delta\bar{r}_k}\right)\Phi_{k-1} -\left(\frac{\varepsilon_{k-0.5}}{\Delta\bar{r}_k\cdot\Delta r_{k-1}}+\frac{\varepsilon_{k+0.5}}{\Delta\bar{r}_k\cdot\Delta r_k}\right)\Phi_k +\left(\frac{\varepsilon_{k+0.5}}{\Delta\bar{r}_k\cdot\Delta r_k}+\frac{\varepsilon_k}{2r_k\Delta\bar{r}_k}\right)\Phi_{k+1} =-q\cdot\rho(r_k) \tag{8}$$

$$\left(-\frac{\hbar^2}{2\cdot m_{k-0.5}\cdot\Delta\bar{r}_k\cdot\Delta r_{k-1}}+\frac{\hbar^2}{4\cdot m_k\cdot r_k\cdot\Delta\bar{r}_k}\right)\Psi_{k-1} +\left(\frac{\hbar^2}{2\cdot m_{k-0.5}\cdot\Delta\bar{r}_k\cdot\Delta r_{k-1}}+\frac{\hbar^2}{2\cdot m_{k+0.5}\cdot\Delta\bar{r}_k\cdot\Delta r_k}+q\cdot\Phi\right)\Psi_k +\left(-\frac{\hbar^2}{2\cdot m_{k+0.5}\cdot\Delta\bar{r}_k\cdot\Delta r_k}-\frac{\hbar^2}{4\cdot m_k\cdot r_k\cdot\Delta\bar{r}_k}\right)\Psi_{k+1} =E\cdot\Psi_k \tag{9}$$

where

$$\varepsilon_{k-0.5}=\frac{\varepsilon_k+\varepsilon_{k-1}}{2},\quad \varepsilon_{k+0.5}=\frac{\varepsilon_{k+1}+\varepsilon_k}{2},\quad \Delta\bar{r}_k =\frac{\Delta r_k+\Delta r_{k-1}}{2} \tag{10}$$

$$\frac{1}{m_{k-0.5}}=\frac{\frac{1}{m_k}+\frac{1}{m_{k-1}}}{2},\frac{1}{m_{k+0.5}}=\frac{\frac{1}{m_{k+1}}+\frac{1}{m_k}}{2}. \tag{11}$$

The carrier distribution is calculated by

$$n(r)=\sum 2m_{\mathrm{d}}D_{\mathrm{p}}(E)\sum\ln\left[1+e^{(E_F-E)/kT}\right]\Psi(r)^2 \tag{12}$$

where the factor of two is due to the fact that Pauli exclusion principle allows two electrons per energy level: one spin up and another spin down, and m_{d} is the density-of-states effective mass.

In the ALTRAS-CNFET, it requires a simultaneous or self-consistent solution to Schrödinger and Poisson equations which are carried out using the Newton-Raphson iterative procedure. At the beginning of the iteration, the sub-band energy and its corresponding wave function are initially calculated by Equation (9). Equation (12) is then employed to calculate the carrier spatial distribution. The resultant potential profile and charge distribution are put to calculate the delta-potential by Newton-Raphson method. The iteration process has to be repeated till the calculated delta-potential is smaller than the tolerance specified by the user, i.e. the calculated potential is sufficiently close to the previous value.

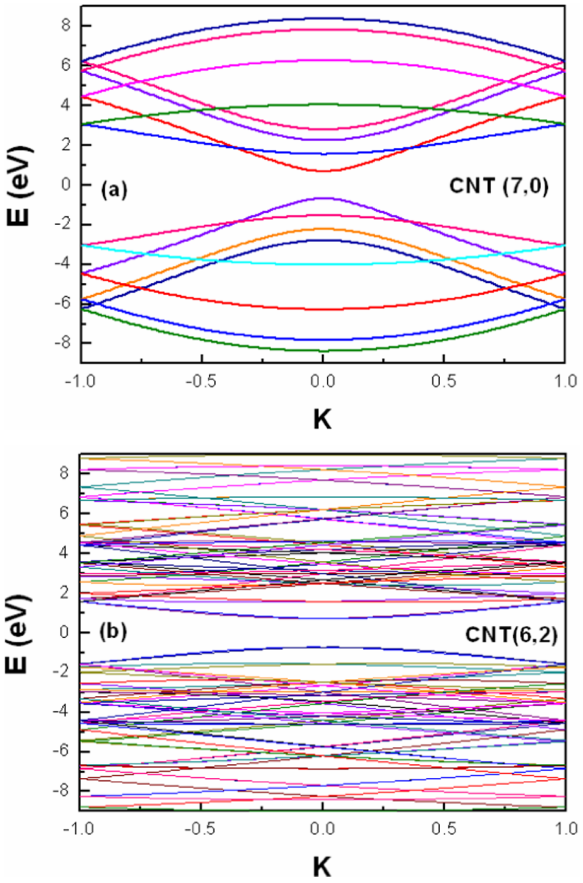

Figure 3. The band structure of two semiconducting CNTs specified by (a) (7, 0) and (b) (6, 2).

The boundary conditions implemented in the simulator are expressed as

$$\left.\frac{\mathrm{d}\phi}{\mathrm{d}r}\right|_{r=0} = 0 \quad \text{and} \quad \phi|_{r=R+T_{\mathrm{ox}}} = \phi_s \tag{13}$$

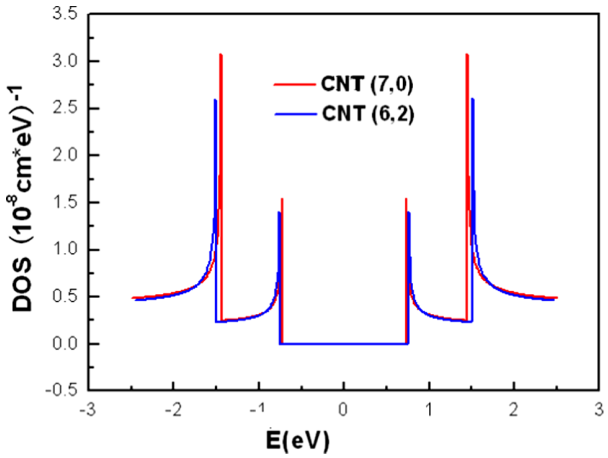

Figure 4. The dependence of density of state on energy for two semiconducting CNTs specified by (7, 0) and (6, 2).

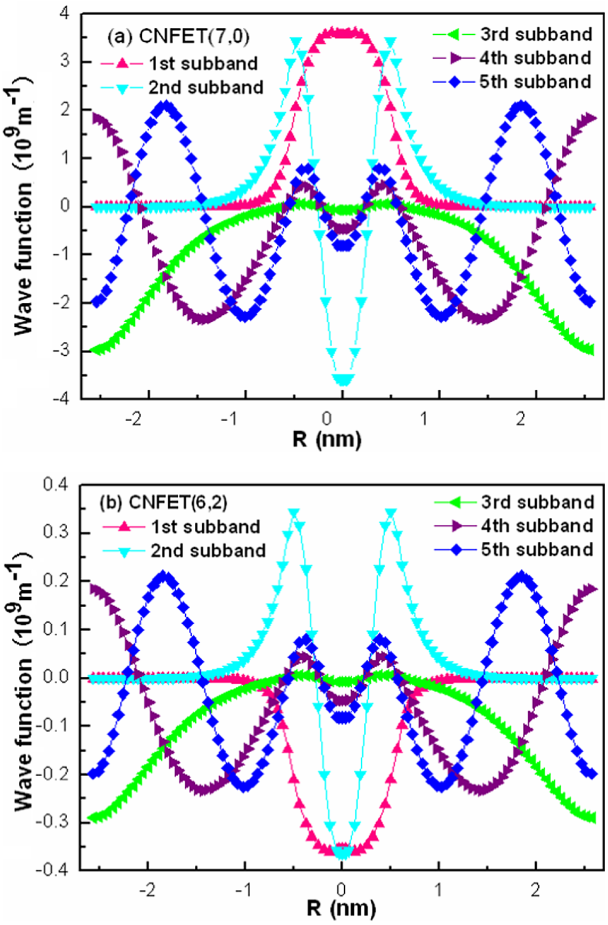

Figure 5. Plots of the wave functions for first few sub-bands, (a) CNFET (7, 0) and (b) CNFET (6, 2).

where R is the radius of CNFET and T_{ox} is the oxide thickness. After reaching convergence condition, the carrier concentration is obtained to compute the direct tunneling gate current quantum mechanically in the radial direction based on tunneling theory [22].

In the gate electrode, the wave function is treated as a traveling plane wave, which can be expressed into the following equation

$$\Psi_{-1} = \exp(ik\Delta x_{-1})\Psi_0 \tag{14}$$

where Δx_{-1} is the uniform mesh spacing between the grid points. The probability current density can be obtained as

$$P_j = \frac{\hbar}{i2m_{\mathrm{g}}}\left(\Psi_j^* \cdot \frac{\partial \Psi_j}{\partial x} - \frac{\partial \Psi_j^*}{\partial x} \cdot \Psi_j\right) \tag{15}$$

which is used to calculate the gate tunneling current density

$$J_{\mathrm{G}} = -q\sum_j N_j^{\mathrm{inv}} P_j. \tag{16}$$

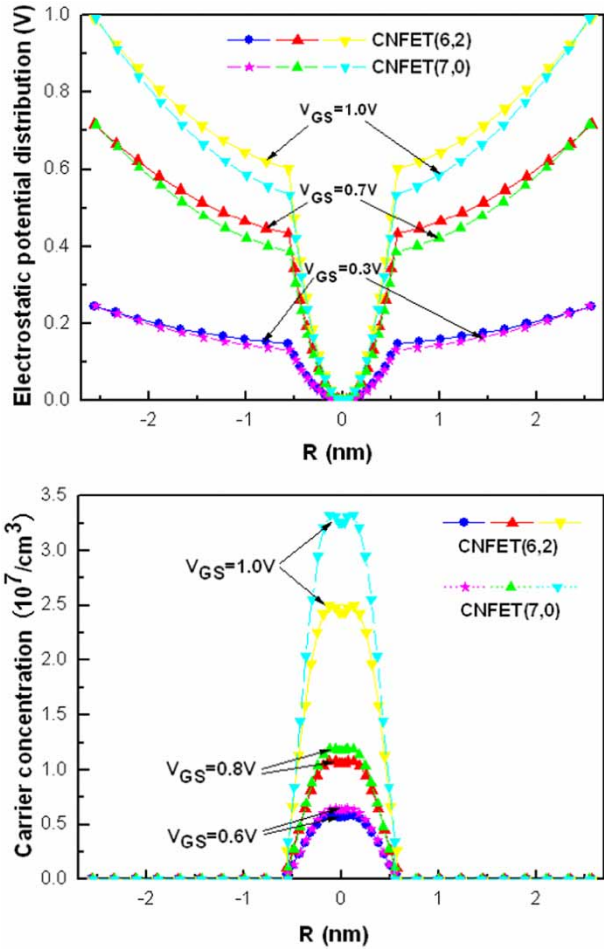

Figure 6. Plot of the electrostatic potential distribution in the radial direction of the two CNFETs when V_{GS} is 0.3, 0.7 and 1 V, respectively.

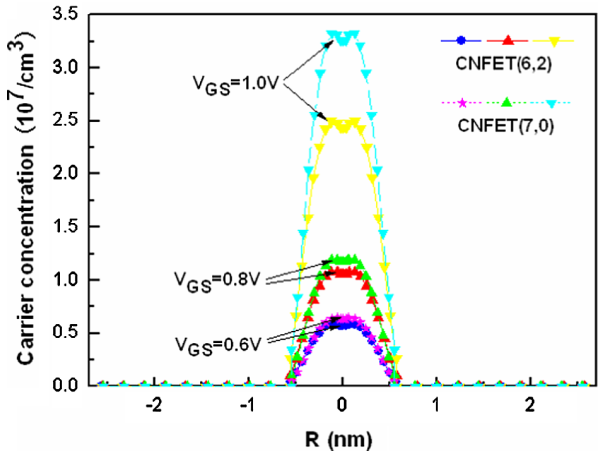

Figure 7. Plot of the carrier distribution in the radial direction of the two CNFETs when V_{GS} is 0.6, 0.8 and 1 V, respectively.

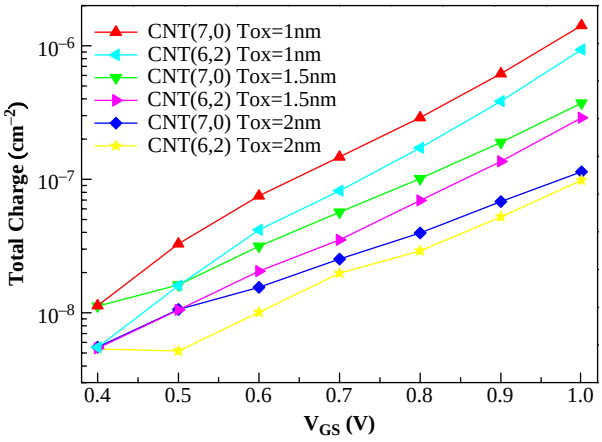

Figure 8. Plot of the total charge versus the gate voltage of the two coaxial CNFETs for three different oxide thicknesses: 1, 1.5 and 2 nm. V_{GS} is from 0.4 to 1.0 V with a step size of 0.1 V.

By substituting Equation (14) into (15), the gate tunneling current density (16) can be calculated quantum mechanically following [22]

$$J_G = q\sum_j N_j^{inv}\sqrt{2(E-E_g)/m_g}\Psi_{0,j}^2 \qquad (17)$$

where N_j^{inv} is the total inversion charge density in each energy level j, E_g and m_g are the conduction band edge and effective carrier mass in the gate electrode, respectively.

2.3 Electrical characteristic in the channel direction of CNFET

In the meantime, according to the theory of ballistic transport, the electrical characteristics of conventional

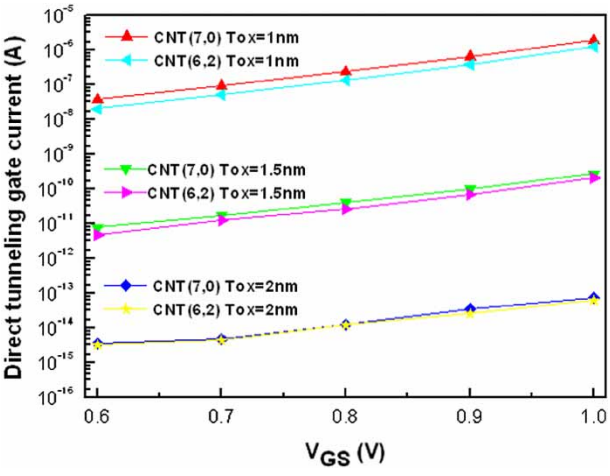

Figure 9. Plot of the direct tunneling gate current versus the gate voltage of the two coaxial CNFETs for three different oxide thicknesses: 1, 1.5 and 2 nm. V_{GS} is from 0.6 to 1.0 V with a step size of 0.1 V.

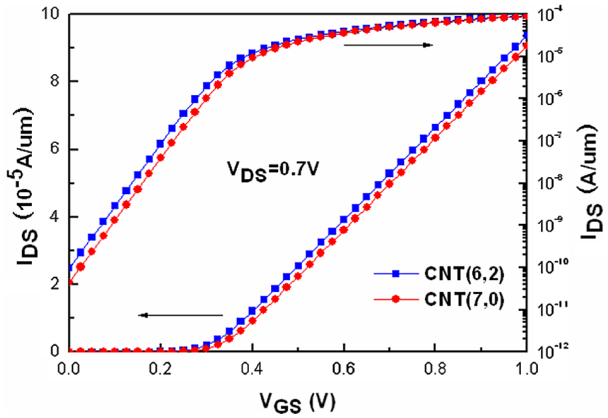

Figure 10. Plot of I_{DS} versus V_{GS} of the two coaxial CNFETs linearly and logarithmically when V_{DS} is 0.7 V.

coaxial CNFETs are implemented effectively in the channel direction. Based on [23–25], it is assumed that the source Fermi level is the reference potential and immediately $\mu_S = 0$ and $\mu_D = -qV_{DS}$ are obtained. It should be noted that only the first sub-band is contained in the simulation. As a consequence, the total drain current I_D in the CNT channel direction can be analytically expressed as

$$I_{DS} = \frac{4qk_BT}{h}\sum\left[\ln\frac{1+e^{(E+U_t-E_F)/kT}}{1+e^{(E+U_t-qV_{DS}-E_F)/kT}}\right] \quad (18)$$

where q is the electronic charge, k_B is the Boltzmann constant, h is the Plank constant, T is the temperature and U_t is the electrostatic potential at the top of barrier.

Since it is known that there is a relation between the mobile charge and electrostatic potential, the quantum

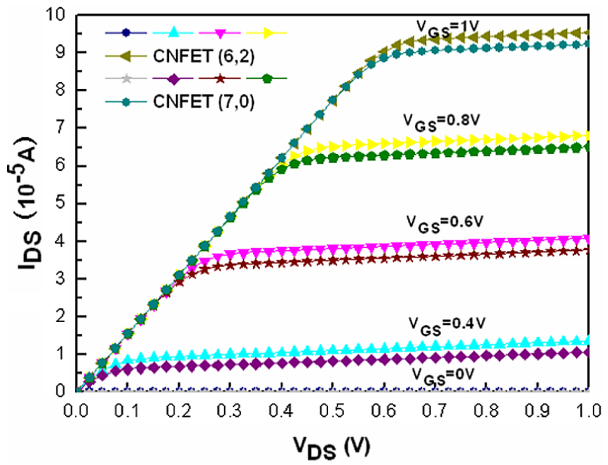

Figure 11. Plot of I_{DS} versus V_{DS} for different V_{GS} of the two coaxial CNFETs. V_{GS} is from 0 to 1 V with a step size of 0.2 V.

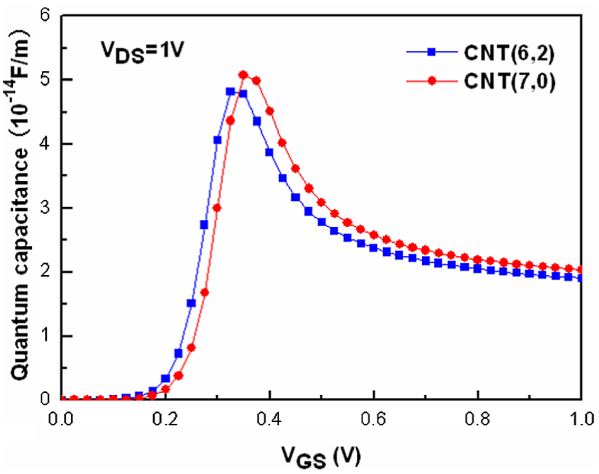

Figure 12. Plot of the quantum capacitance versus V_{GS} of the two coaxial CNFETs when V_{DS} is 1 V.

capacitance can be calculated by

$$C_Q = -q^2\frac{\partial(N_m)}{\partial(U_t)} \quad (19)$$

where N_m is the mobile charge, which is dependent on the potential at the top of the barrier.

From the perspective of the MOSFET device physics, the voltage gain and sub-threshold swing are also obtained accurately according to Equations (20) and (21), respectively.

$$A_V = \frac{g_m}{g_d} = \frac{\partial I_D/\partial V_{GS}}{\partial I_D/\partial V_{DS}} \quad (20)$$

$$S \approx \frac{\partial V_{GS}}{\partial \log(I_{DS})}. \quad (21)$$

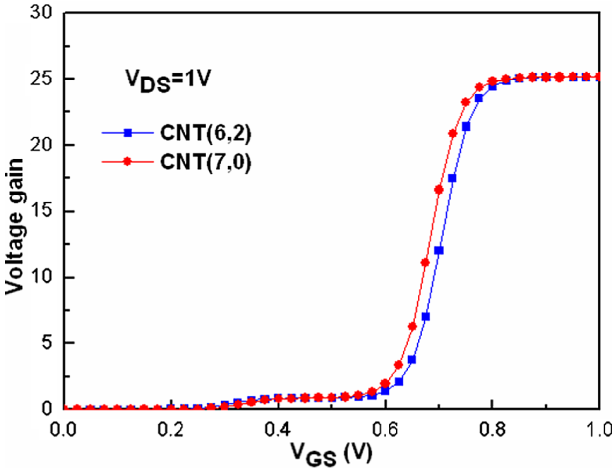

Figure 13. Plot of the voltage gain as a function of gate voltage of the two coaxial CNFETs when V_{DS} is 1 V.

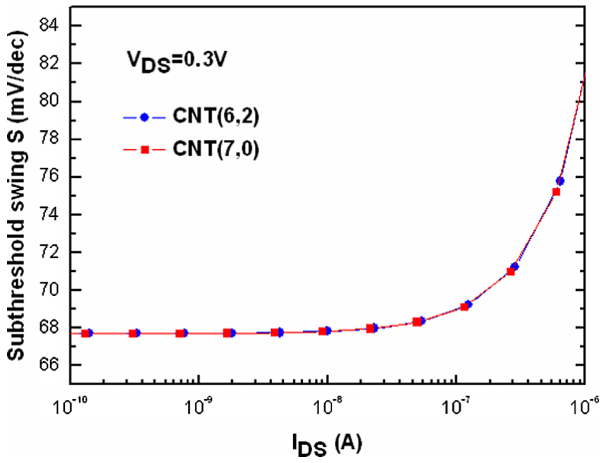

Figure 14. Plot of the extracted sub-threshold swing from the output characteristic as a function of I_{DS} for the two coaxial CNFETs when V_{DS} is 0.3 V.

3. Results and discussion

In order to test the validity of the ALTRAS-CNFET simulator, two semiconducting CNTs specified by (7, 0) and (6, 2) were fed into this simulator. As a result, comparing with the model without considering curvature effects, better band structure diagram is obtained and shown in Figure 3. The density of states is calculated correctly in Figure 4. After the self-consistent calculation, the plots of the wave functions of the two CNFETs for first few sub-bands are shown in Figure 5.

The Poisson equation relates the second-order derivative of the potential distribution to the charge concentration at every radial point within the domain of interest. The resultant electrostatic potential distribution in the radial direction is illustrated in Figure 6 when V_{GS} is 0.3, 0.7 and 1 V, respectively. Simultaneously the carrier distribution in the radial direction is shown in Figure 7 when V_{GS} is 0.6, 0.8 and 1 V, respectively.

The plot of the total charge versus the gate voltage of the two coaxial CNFETs is shown in Figure 8 for three different oxide thicknesses: 1, 1.5 and 2 nm when V_{GS} is from 0.4 to 1.0 V with a step size of 0.1 V. The dependence of direct tunneling gate current on the gate voltage for different oxide thickness is plotted in Figure 9 for different oxide thicknesses. It is obviously shown that an increase in the drain current with a drop in the oxide thickness, which is ascribed to the increase of the induced charge due to the thinner oxide layer. It is worthy to note that the high-*K* dielectric lends itself to lower the gate tunneling [25]. The plots of I_{DS} versus V_{GS} and I_{DS} versus V_{DS} are shown in Figures 10 and 11, respectively. The accurate transfer and output characteristics are similar with those of the conventional silicon devices. Figures 12–14 are the obtained quantum capacitance versus V_{GS}, voltage gain versus V_{GS}, and sub-threshold swing versus I_{DS}, respectively, from ALTRAS-CNFET. These results coincide with the previous theory prediction and can be used to design and optimize the electrical characteristics of CNFETs.

From the device simulation point of view, such a powerful simulator is easy-to-use and does not require highly computational resources and time consumption. All the obtained results of CNT (7, 0) are similar with those of CNT (6, 2), because the two CNTs are both semiconductors without large differences on the material characteristics. The use of high-*K* gate dielectrics leads to higher induced charge in the channel, which can remarkably lower the gate tunneling and the parasitic capacitance between the gate and the source (and drain). The low quantum capacitance and sub-threshold swing effectively perform the excellent properties of CNFETs. However, only the first sub-band is contained in the simulator, which results in the applied gate voltage being confined in the low range. As the gate bias increases and the energy band moves down, the sub-bands are populated one after the other. It is necessary to extend it into all the populated sub-bands in order to gain large ranges of gate bias, which will be the future work.

4. Summary and conclusions

In summary, ALTRAS-CNFET is a powerful tool for CNT energy-band calculation and CNFET performance prediction. It can directly compute the gate tunneling current in the radial direction, drain current in the channel and other electrical characteristics correctly based on device geometry and CNT material characteristics. The predicted results indicate that CNT is the most promising successor to silicon and the coaxial CNFET is likely to operate excellently.

Acknowledgements

This work is subsided by the special funds for major state basic research project (973) and the Nature Science Funds of China (90607017). This work is also partially support by an Earmarked Grant from the Research Grant Council of Hong Kong SAR and a NEDO grant from Japan.

References

[1] ITRS, *International technology roadmap for semiconductors 2005 edition Emerging research devices (includes emerging research materials)*, Website: http://www.itrs.org.
[2] P. Avouris, J. Appenzeller, R. Martel, and S.J. Wind, *Carbon nanotube electronics*, Proc. IEEE 91(11) (2003), pp. 1772–1784.
[3] P.L. McEuen, M.S. Fuhrer, and H. Park, *Single-walled carbon nanotube electronics*, IEEE Trans. Nanotechnol. 1 (2002), pp. 78–85.
[4] P.G. Collins and P. Avouris, *Nanotubes for electronics*, Sci. Am. (2000), pp. 62–69.

[5] R. Saito, G. Dresselhaus, and M.S. Dresselhaus, *Physical properties of carbon nanotubes*, Carbon 33(7) (1995), pp. 883–891.
[6] J.W. Mintmire and C.T. White, *Universal density of states for carbon nanotubes*, Phys. Rev. Lett. 81(12) (1998), pp. 2506–2509.
[7] X. Wang, *Research on Carbon Nanotube Field-effect Transistors and Related Basic Problems*, Doctor Dissertation, Peking University, 2004.
[8] F. Leonard and J. Tersoff, *Dielectric response of semiconducting carbon nanotubes*, Appl. Phys. Lett. 81(25) (2002), pp. 4835–4837.
[9] Y.M. Niquet, C. Delerue, G. Allan, and M. Lannoo, *Method for tight-binding parametrization: application to silicon nanostructures*, Phys. Rev. B 62(8) (2000), pp. 5109–5116.
[10] L. Yang, M.P. Anantram, and J.P. Lu, *Band-gap change of carbon nanotubes: effect of small uniaxial and torsional strain*, Phys. Rev. B 60(29) (1999), pp. 13874–13878.
[11] A. Raychowdhury, S. Mukhopadhyay, and K. Roy, *A circuit-compatible model of ballistic carbon nanotube field-effect transistors*, IEEE Trans. Comput. Aided Des. Integr. Circ. Syst. 23(10) (2004), pp. 1411–1420.
[12] B.C. Paul, S. Fujita, M. Okajima, and T. Lee, *A compact model of ballistic CNFET for circuit simulation*, NSTI-Nanotech 3 (2006), www.nsti.org, ISBN 0-9767985-8-1.
[13] J. Knoch, S. Mantl, and J. Appenzeller, *Comparison of transport properties in carbon nanotube field-effect transistors with Schottky contacts and doped source/drain contacts*, Solid-state Electron. 49(1) (2005), pp. 73–76.
[14] M. Pourfath, H. Kosina, and S. Selberherr, *Rigorous modeling of carbon nanotube transistors*, J. Phys. Conf. Ser. 38 (2006), pp. 29–32.
[15] J. Guo, S. Datta, M. Lundstrom, and M.P. Anantam, *Towards multi-scale modeling of carbon nanotube transistors*, Int. J. Multiscale Comp. Eng. 2 (2004), p. 60. e-print cond-mat/0312551.
[16] D.L. John, L.C. Castro, J. Clifford, and D.L. Pulfrey, *Electrostatics of coaxial Schottky-barrier nanotube field-effect transistors*, IEEE Trans. Nanotechnol. 2(3) (2003), pp. 175–180.
[17] S. Heinze, J. Tersoff, and P. Avouris, *Electrostatic engineering of nanotube transistors for improved performance*, Appl. Phys. Lett. 83(24) (2003), pp. 5038–5040.
[18] Jason P. Clifford, D.L. John, Leonardo C. Castro, and D.L. Pulfrey, *Electrostatics of partially gated carbon nanotube FETs*, IEEE Trans. Nanotechnol. 3(2) (2004), pp. 281–286.
[19] J. Guo, J. Wang, E. Polizzi, S. Datta, and M. Lundstrom, *Electrostatics of nanowire transistors*, IEEE Trans. Nanotechnol. 2 (2003), pp. 329–334.
[20] J. Guo, S. Goasguen, M. Lundstrom, and S. Datta, *Metal–insulator–semiconductor electrostatics of carbon nanotubes*, Appl. Phys. Lett. 81(8) (2002), pp. 1486–1488.
[21] J. Appenzeller, R. Martel, V. Derycke, M. Radosavljevic, S. Wind, D. Neumayer, and P. Avouris, *Carbon nanotubes as potential building blocks for future nanoelectronics*, Microelectron. Eng. 64(1–4) (2002), pp. 391–397.
[22] H. Iwata, *Fully quantum-mechanical modeling of tunneling current in ultrathin gate oxide metal–oxide–semiconductor devices*, Jpn. J. Appl. Phys. 40 (2001), pp. 4496–4500.
[23] A. Rahman, J. Guo, S. Datta, and M.S. Lundstrom, *Theory of ballistic nanotransistors*, Trans. Electron Dev. 50(9) (2003), pp. 1853–1864.
[24] A. Javey, J. Guo, Q. Wang, M. Lundstrom, and H. Dai, *Ballistic carbon nanotube field-effect transistors*, Nature 424 (2003), pp. 654–657.
[25] J. Guo, M. Lundstrom, and S. Datta, *Performance projections for ballistic carbon nanotube field-effect transistors*, Appl. Phys. Lett. 80(17) (2002), pp. 3192–3194.
[26] A. Javey, H. Kim, M. Brink, Q. Wang, A. Ural, J. Guo, P. Mcintyre, P. McEuen, Lundstrom, and H. Dai, *High*-K *dielectrics for advanced carbon-nanotube transistors and logic gates*, Nature Mater. 1 (2002), pp. 241–246.